Oxidation of Ordered Sn/Pt(111) Surface Alloys and Thermal Stability of the Oxides Formed

Najat A. Saliba, Yi-Li Tsai, and Bruce E. Koel*

Department of Chemistry, University of Southern California, Los Angeles, California 90089-0482

Received: August 26, 1998; In Final Form: December 2, 1998

Two Pt−Sn surface alloys were oxidized at 300 K by ozone (O_3) exposure in UHV. Both alloys were less reactive than Pt(111), and the p(2 × 2) alloy ($\Theta_{Sn} = 0.25$) was more reactive than the ($\sqrt{3}$x$\sqrt{3}$)R30° alloy ($\Theta_{Sn} = 0.33$). The relative O_3 dissociative sticking coefficients on these surfaces at 300 K were 1.0:0.79:0.33, respectively. Ozone dissociation was inhibited more easily on the alloys than on Pt(111), and large O_3 doses on the p(2 × 2) and ($\sqrt{3}$x$\sqrt{3}$)R30° surface alloys produced oxygen coverages of 1.2 and 0.87 monolayers, respectively, compared to 2.4 monolayers on Pt(111). Both chemisorbed and "oxidic" oxygen states were characterized by using Auger electron spectroscopy (AES), temperature-programmed desorption (TPD), and low-energy electron diffraction (LEED). At 300 K, chemisorbed oxygen adatoms are formed at low exposures, but oxidation of Sn occurs at large oxygen coverages, as evidenced by a 1.6 eV downshift of the Sn(MNN) AES peak. Heating during TPD causes SnO_x formation even at low coverages, and this decomposes to liberate O_2 in desorption peaks at 1015 and 1078 K on the p(2 × 2) and ($\sqrt{3}$x$\sqrt{3}$)R30° surfaces, respectively. After oxidation of Sn, TPD indicates desorption of oxygen from chemisorbed adatoms bound at Pt sites and eventually formation of platinum oxide particles. SnO_x particles formed in intimate contact with Pt by oxidation of these Pt−Sn alloys and high-temperature heating are easier (100 K) to reduce by heating in a vacuum than a corresponding thick SnO_x film. We also find additional stability (130 K) imparted to PtO_x particles by the presence of oxidized Sn following oxidation of these alloys. Heating these oxidized alloys to 1000 K produces a (4 × 1) LEED pattern that we have assigned to the formation of large domains of an SnO_2 overlayer on both of the surface alloys.

Introduction

The selectivity and lifetime of platinum−tin bimetallic catalysts for naphtha reforming[1−4] and various hydrogenation/dehydrogenation reactions[5] are greatly improved over those for platinum catalysts. Pt−Sn catalysts have also been used for oxidation reactions, for example in methanol electrooxidation[6−8] and in low-temperature CO oxidation.[9−16] In this regard, oxidation and reduction of platinum−tin bulk alloys have been studied rather extensively with Auger electron spectroscopy (AES),[17−22] angle-resolved Auger electron spectroscopy (ARES),[23,24] X-ray photoelectron spectroscopy (XPS),[24,25] and ion-scattering spectroscopy (ISS).[21−24] Nonetheless, important details about the interactions of oxygen with Pt−Sn surfaces remain unclear, primarily because the composition of the surfaces of these alloys was found to be affected by the "treatment" applied to the sample, e.g., sputtering with Ar^+ ions and exposure to hydrogen enriched the surface region in Pt, while annealing or exposure to oxygen enriched the surface in Sn.

In oxidation studies of a bulk Pt_3Sn alloy over the temperature range 300−900 K, using O_2 at low pressures (10^{-4}−10^{-3} Pa), Unger and Marton[25] found that the oxygen content of the surface increased monotonically (with little subsurface diffusion) with increasing temperature between 300 and 800 K but decreased at higher temperatures (>920 K) due to oxygen dissolution into the subsurface region and/or desorption. At higher temperatures (500−800 K), an "oxidic" Sn species was thought to be formed via oxygen incorporation, and this interpretation is consistent with the earlier conclusions of Asbury and Hoflund.[23] These authors reported a maximum oxygen uptake with the bulk Pt_3Sn alloy sample held at 470 K during dosing. Both chemisorbed and "oxidic" oxygen species were assigned following oxidation of Pt_3Sn at 470 K, but only the "oxidic" form (attributed to tin oxide) dominated following oxidation at 670 K. In these studies, the chemical state of Pt did not appear to be affected by oxygen uptake under any of these conditions.

In related work on the oxidation of Pd_3Sn, Rotermund et al.[26] developed a model for the phases formed by oxidation over the temperature range 300−1070 K under UHV conditions. The O_2 dissociative sticking coefficient (S) was small and independent of oxygen coverage up to ~0.3 monolayers and independent of temperature. At low temperatures (<520 K) oxygen is associated with Sn in a quasimetallic state (resembling an O−Sn chemisorption state) and a nucleated two-dimensional tin oxide state, with the former favored by low surface mobility of Sn. A "saturation" oxygen coverage of ~0.3 monolayers was reached on Pd_3Sn below 800 K because S decreased rapidly above this coverage due to limited Sn diffusion. Increasing the temperature above 800 K caused the tin oxide state to dominate at the surface at 0.3 monolayers, and S remained constant up to at least 1 monolayer. Strong Sn segregation into the surface region allowed for three-dimensional tin oxide growth at high temperatures.

Determining the oxidation state of tin and the chemical nature of tin oxide formed by oxidation reactions at Sn and alloyed-Sn/TM surfaces has been the subject of numerous studies and

* Corresponding author.

10.1021/jp983523q CCC: $18.00
Published on Web 02/13/1999

is still controversial.[27−41] The tin oxide formed has been identified previously as SnO, SnO_2, a mixture of SnO and SnO_2, an intermediate oxide phase (first identified by Cox and Hoflund using ELS[32]), and a phase different from SnO or SnO_2.[37] The controversy arises because of difficulties in preparing standards and the range of chemical shifts that have been reported in XPS of the Sn($3d_{5/2}$) core level peak between the Sn^{2+} and Sn^{4+} oxides.[36,39,41] Also, there is almost a 7 eV spread in the reported AES chemical shifts of the main Sn(MNN) peak at 430 eV KE from tin metal to the oxide.[30] This issue was presumably resolved by Gagiotti et al.[38] who assigned 485.4 eV BE to SnO and 486.7 eV BE to SnO_2, but even these assignments have been called into question.[40,41]

Our experiments extend those done previously in two significant ways by using well-characterized Pt−Sn surface alloys and ozone (O_3) as the oxidant. Studies of the oxidation of these two surface alloys minimizes the interference of Sn adatoms and bulk Sn on the results. Ozone, a very reactive molecule, was used as a clean and efficient oxygen source in UHV to carry out extensive oxidation at 300 K with no H_2O coadsorption.[42] No dissociative O_2 chemisorption occurs on the (2×2)-Sn/Pt(111) and $(\sqrt{3}x\sqrt{3})R30°$-Sn/Pt(111) surface alloys under UHV conditions.[43]

Ozone has been used several times in our laboratory for oxidation studies of noble metals such as Au(111),[44] and Pt(111)[45] and(100).[46] Ozone exposures on Au(111)[44] at 300 K formed oxygen adatoms with a maximum coverage of $\Theta_o = 1.2$, disordering the surface and possibly forming Au_xO_y oxidic species. On Pt(111)[45] and Pt(100),[46] we identified both chemisorbed and oxidic states of oxygen. The chemisorbed state (oxygen adatoms) desorbed in broad O_2 TPD peaks which shifted to lower temperature with increasing oxygen coverages, whereas oxygen desorption from platinum oxides were characterized by sharp and narrow O_2 TPD peaks at 660 K for Pt(100)[46] and 708 K for Pt(111)[45] at high coverages. The assignment of this O_2 evolution to platinum oxide decomposition is consistent with older work by Sales et al.[47] in which they reported platinum oxide decomposition on an oxidized polycrystalline Pt wire between 670 and 840 K at 1 atm. These authors also questioned finding "oxides" at higher temperatures and lower pressures[48,49] since PtO_x is known to be thermodynamically unstable at temperatures above 650 K. In work very complementary to that described herein, we report elsewhere oxidation of Sn/Pt(100) surface alloys[50,51] using O_3 under UHV conditions. This oxidation lead to the formation of a tin oxide overlayer with only a small amount of platinum oxidation. The formation of SnO_x from the surface alloys was indicated by a similarity in the O_2 evolution temperature from thick layers of SnO_x, and the XPS results confirmed the formation of tin oxide (SnO_x) at temperatures higher than 770 K.

Experimental Procedures

The experiments were carried out in a two-level, stainless steel UHV chamber described previously,[52] with a base pressure of 1.5×10^{-10} Torr. Briefly, it is equipped with a shielded quadrupole mass spectrometer (QMS) for TPD mass spectrometry, double-pass cylindrical mirror analyzer (CMA) for AES, four-grid LEED optics, and directed beam gas dosers using microcapillary arrays.

TPD measurements were made using the QMS ionizer in line of sight with the sample surface and using a linear heating rate of 4 K/s. Absolute oxygen coverages in these experiments were determined by comparing O_2 TPD peak areas following ozone exposures to those from O_2 exposures on Pt(111) at 300 K which gives a saturation coverage of $\Theta_o = 0.25$.[53] All coverages (Θ) in this paper are reported in monolayers referenced to the Pt(111) surface atom density ($\Theta = 1.0$ for 1.5×10^{15} cm^{-2}).

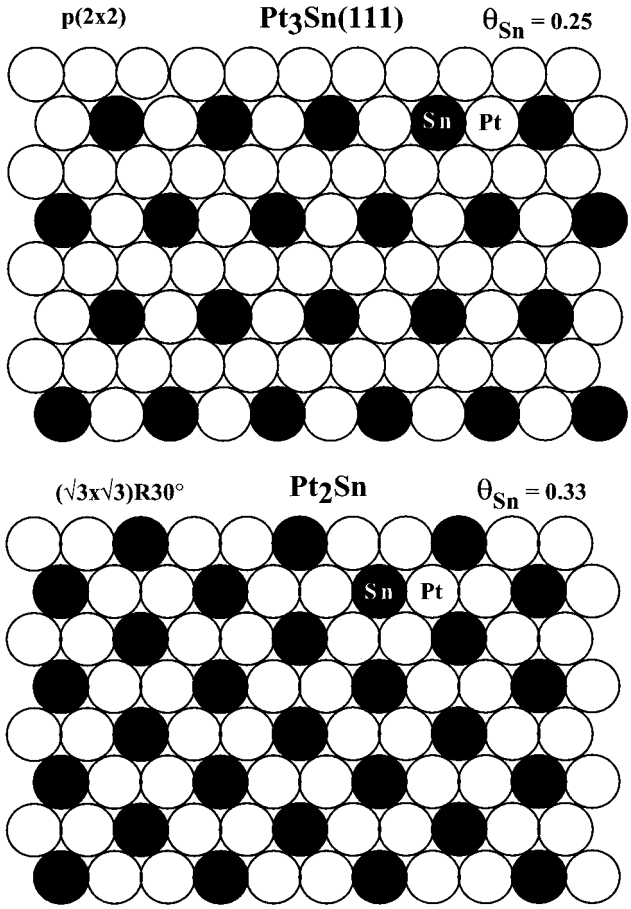

Figure 1. Schematic of the real space structure of the (2×2)- and the $(\sqrt{3}x\sqrt{3})R30°$-Sn/Pt(111) surface alloys.

The Pt(111) crystal was suspended between two 20-mil Ta wires and could be cooled to 100 K using liquid nitrogen or resistively heated to 1200 K. The temperature was measured by a chromel−alumel thermocouple spot welded to the side of the crystal. The Pt(111) single-crystal surface was cleaned in the chamber by a combination of Ar^+ ion sputtering at 300 K, annealing in a vacuum at 1200 K, and oxygen treatments (1×10^{-8} Torr O_2) with the sample at 1000 K.

The (2×2)-Sn/Pt(111) and $(\sqrt{3}x\sqrt{3})R30°$-Sn/Pt(111) surface alloys, with surface stoichiometries of Pt_3Sn and Pt_2Sn, respectively, are shown in Figure 1. These were prepared following the procedure used by Paffett and Windham[54] via evaporation of either ~0.7 or ~0.9 monolayers of Sn onto the Pt(111) single crystal at 300 K (with the smaller amount used for the (2×2) surface alloy) and then annealing the crystal at 1000 K for 10 s. Both of these surface alloys have now been studied by angle-dependent low-energy ion-scattering spectroscopy (LEISS),[55] LEED I-V,[56] and X-ray photoelectron diffraction (XPD)[57] with the conclusion that Sn is incorporated into the Pt surface layer to form a substitutional surface alloy with the Sn atoms almost coplanar with the Pt top-layer atoms; protruding about 0.2 Å above the surface Pt plane. For simplicity later in the text, we will use the notations (2×2) and $\sqrt{3}$ for the (2×2)-Sn/Pt(111) and $(\sqrt{3}x\sqrt{3})R30°$-Sn/Pt(111) surface alloys, respectively.

Ozone (O_3) was prepared in our laboratory using a commercial ozone generator and concentrated on a silica gel trap. The effluent gas from the generator contained a mixture of

approximately 5% ozone and 95% unreacted O_2. This mixture was passed through a gas absorption bottle containing dried silica gel suspended in a dewar filled with an ethanol−dry ice bath at −80 °C. This process was carried out for several hours to obtain saturation of the silica gel with ozone. The ozone may be kept indefinitely at −80 °C, but we warn users that there is always a chance of explosion if it is allowed to warm or accidentally come in contact with the ethanol in the bath. The O_2 impurity was removed by cooling the trap to −110 °C and pumping with a mechanical pump. The trap was then allowed to warm to −80 °C. Because ozone is such a reactive molecule, it was necessary to rigorously passivate the stainless steel gas handling line and any copper components (e.g., gaskets) by flushing the lines several times with ozone. We found that ozone still decomposed in the lines over a period of minutes, and therefore it was necessary to recharge the lines frequently. A glass microcapillary array doser was connected to the leak valve on the chamber and was used for dosing ozone directly onto the sample. A mass spectrum of the background gases in the UHV chamber during ozone dosing showed primarily a large signal at 32 amu (O_2), and only small signals of ∼ 10% at 28 amu (CO) and 1% at 18 amu (H_2O) because of wall and filament reactions.

All ozone dosing was performed with the Pt(111) crystal at 300 K. In addition, picking an exposure temperature and maintaining this value is important because the saturation oxygen coverage depends on the exposure temperature. Exposures are given in arbitrary units of Langmuirs (L) as determined by the background gas pressure in the chamber during dosing without any further corrections.

Results

O_3 Adsorption on Pt(111). Some of the results for O_3 adsorption on Pt(111)[45] are briefly reviewed here to provide a reference for the studies reported on Sn/Pt(111) surface alloys. O_3 dissociatively adsorbed on Pt(111) at 300 K with a value for the initial sticking coefficient of $S_0 \geq 0.24$. This may be compared to that for O_2 on Pt(111) at 300 K with a dissociative sticking coefficient of $S_0 \sim 0.05$.[58−60] Both O_2 and O_3 exposures lead to a (2 × 2)-O LEED pattern at $\Theta_O \sim 0.25$, but O_3 reaction leads readily to higher oxygen coverages and even platinum oxide layers under UHV conditions. As shown in Figure 2, the thermal desorption profiles of O_2 after O_3 exposures on Pt(111) at 300 K change markedly depending on Θ_O. For $\Theta_O < 0.32$, the O_2 TPD peak is symmetric with a maximum that shifts from 814 to 742 K as the coverage increases, consistent with second-order kinetics. For $0.32 \leq \Theta_O \leq 0.95$, the O_2 TPD profile broadens considerably to lower temperature, with a feature 558 K developed for $\Theta_O > 0.54$. However, the behavior of the O_2 TPD peaks for $\Theta_O > 0.95$ changes, signaling formation of small particles of platinum oxide. First, the peaks shift to higher temperature with increasing coverage. Second, an unusual "undercutting" of the leading edges of the peaks indicates that the desorption rate is not a unique function of Θ_O, possibly because of strong attractive interactions. The small oxide particles formed at 300 K decompose to liberate O_2 between 634 and 708 K. Oxidation of Pt(111) in this manner is reversible, and all of the oxygen desorbs during subsequent heating in TPD. Furthermore, oxygen does not penetrate deep into the bulk at 300 K. [45]

O_3 Adsorption on Sn/Pt(111) Surface Alloys. *TPD Studies*. Figure 3 shows the O_2 TPD curves obtained after O_3 exposures on the (2 × 2) alloy at 300 K. At the lowest coverage studied, $\Theta_O = 0.03$, O_2 desorption first occurs in a peak at 960 K. At

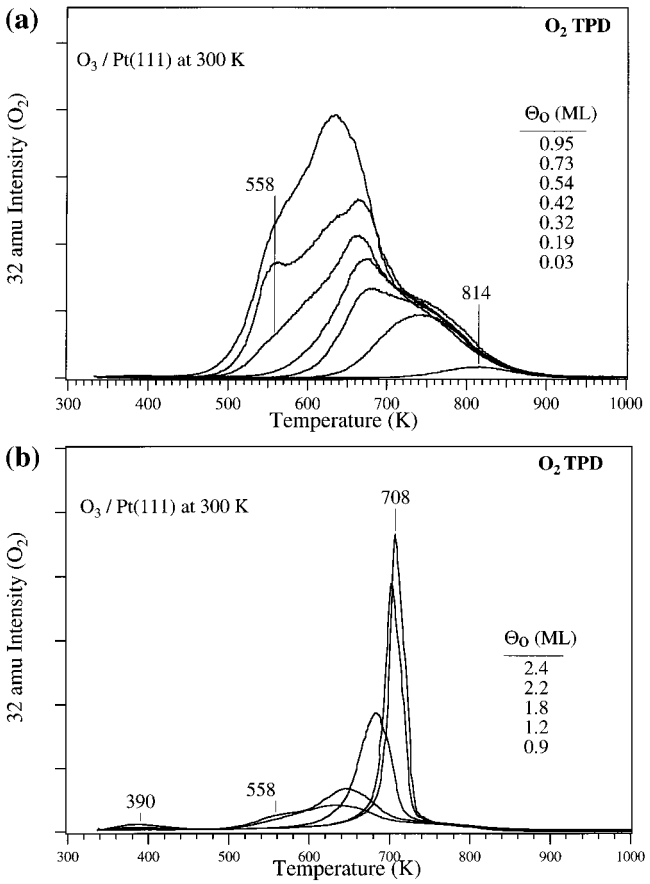

Figure 2. O_2 TPD curves following O_3 exposures of 0.1−1 L (a) and 1−20 L (b) on Pt(111) at 300 K.

higher coverages, this high-temperature feature shifts to 1015 K. When $\Theta_O \geq 0.3$, the amount of O_2 desorption in the high-temperature feature does not increase further, but the O_2 desorption profile broadens greatly to lower temperature and another peak appears at 775 K. Even higher oxygen coverages first form a low-temperature feature at near 730 K, but for $\Theta_O \geq 1.0$ this broad profile coalesces and shifts to higher temperatures. Notably, the undercutting of the peak leading edges is reminiscent of our previous observations on Pt(111) and the formation of PtO_x,[45] but the sharp O_2 peak occurs at about 110 K higher temperature here, i.e., at 820 K compared to 708 K on Pt(111).

Figure 4 shows O_2 TPD spectra following O_3 exposure on the $\sqrt{3}$ alloy at 300 K. O_2 desorption is clearly separated into two regions: desorption above 950 K and desorption from 600 to 900 K. At the lowest oxygen coverage studied, $\Theta_O = 0.002$, a single desorption peak is observed at 1002 K. This peak shifts to higher temperature with increasing oxygen coverage until reaching 1078 K at the highest coverages. Both the shape and the increase in the desorption temperature of the peaks as the coverage increases indicate fractional- or zero-order desorption kinetics. Analysis of the high-temperature portions of the TPD curves for $0.002 \leq \Theta_O \leq 0.15$ utilizing the method of Parker et al.[61] indicates one-half-order desorption kinetics with $E^d = 88-86$ kcal/mol. At coverages higher than $\Theta_O = 0.1$, O_2 desorption starts to occur at lower temperatures, first at 760 K and then in curves for $\Theta_O = 0.5$ and 0.73, another feature appears at 730 K. For $\Theta_O \geq 0.83$, the main peak desorption temperature now increases from 750 to 834 K as the oxygen coverage increases and the profiles in this temperature range show undercutting of the TPD curves.

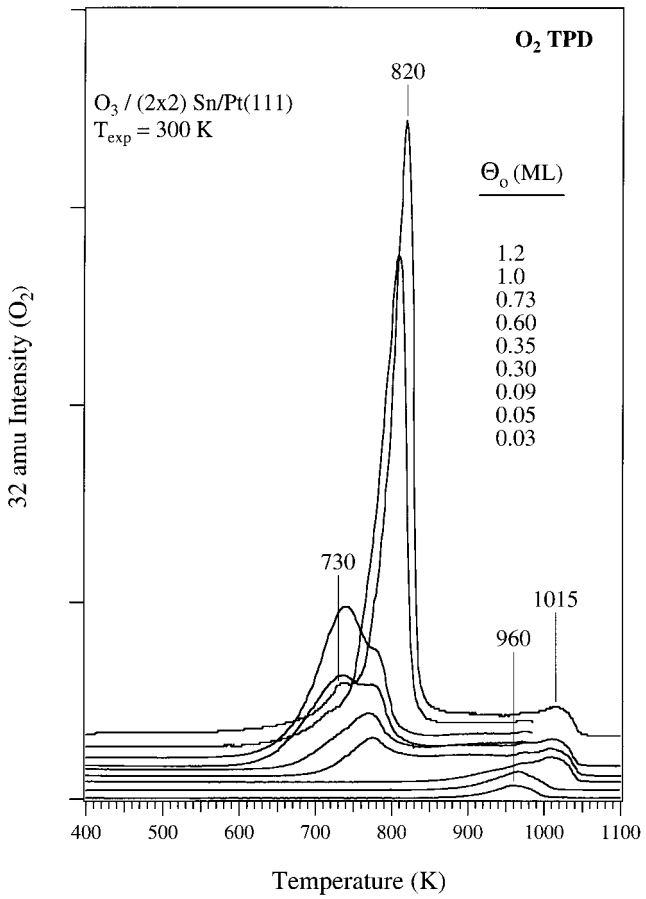

Figure 3. O_2 TPD curves following O_3 exposures of 0.05−8 L on the (2 × 2)-Sn/Pt(111) alloy at 300 K.

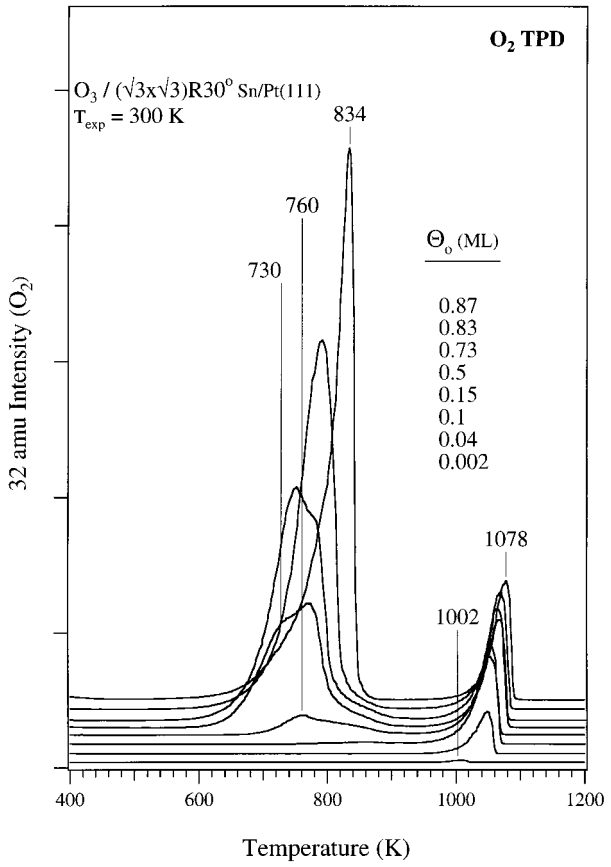

Figure 4. O_2 TPD curves following O_3 exposures of 0.05−8 L on ($\sqrt{3}$x$\sqrt{3}$)R30°-Sn/Pt(111) alloy at 300 K.

Figure 5 utilizes O_2 TPD peak areas of the O_2 TPD spectra of Figures 2 − 4 to quantitate oxygen uptake on these three surfaces. On Pt(111), a saturation coverage of $\Theta_O^{sat} = 2.4$ is reached after an O_3 exposure of 20 L. An exposure of 8 L O_3 on the (2 × 2) alloy is sufficient to reach a saturation coverage of $\Theta_O^{sat} = 1.2$. For the $\sqrt{3}$ alloy, a saturation coverage of $\Theta_O^{sat} = 0.87$ is reached after 6 L O_3 exposure. The initial slopes of these uptake curves correspond to the initial dissociative sticking coefficient, S_0, of ozone on these surfaces, and differentiation of these curves provides the value of the dissociative sticking coefficient, S, as a function of Θ_O. Surface Sn decreases S_0, such that $S_0 = 0.24$, 0.19, and 0.08 on the Pt(111), (2 × 2) alloy, and $\sqrt{3}$ alloy surfaces, respectively. The $S(\Theta_O)$ curves on all three surfaces are described very well by functions of the form $S(\Theta_O) = S_0(1 - a\Theta_O)$, where $a = 0.42$, 0.67, and 1.06 on the three surfaces, respectively, with increasing Sn concentration. Thus, both the sticking coefficient and the saturation oxygen concentration at 300 K *decrease* with increasing amounts of surface Sn in the Pt−Sn alloys. This result is contrary to naïve expectations, and points to the importance of alloy studies because of their often surprising chemistry. The surface structure and composition of the Pt−Sn alloys is crucial in determining this chemistry, and we find, for example, that oxidation of Sn/Pt(100) surface alloys[50,51] using O_3 under UHV conditions is *enhanced* over that of the Pt(100) surface.

AES Studies. Characterization of the oxygen uptake by AES after ozone exposures on the (2 × 2) alloy at 300 K is shown in Figure 6a,b. On the (2 × 2) alloy, the O(506) signal increases linearly with O_3 exposure until at least $\Theta_O = 0.7$. Both Sn(430) and Pt(237) signals appear to be unchanged until about $\Theta_O >$ 0.09, but by $\Theta_O = 0.7$ the Pt signal is attenuated to a greater extent than is Sn and so the Sn/Pt ratio increases. Saturation is effectively reached for all of the AES signals after 4 L O_3.

Additional chemical information is available if we look carefully at the AES peak positions during oxygen uptake, as shown in Figure 6b. Small amounts of oxygen, in the range where the Sn and Pt signals are roughly constant, do not affect the kinetic energy of the Sn(MNN) peak, but at large concentrations, at least by $\Theta_O = 0.6$, this Sn peak shifts lower by 1.6 eV. The O(KVV) and the Pt(NNO) peak positions never shift appreciably. We interpret the shift in the Sn(MNN) peak as a signal for Sn oxidation that occurs for $\Theta_O \geq 0.6$ on the (2 × 2) alloy at 300 K (Sn oxidation refers to the formation of a strong Sn−O interaction that is not yet representative of an "oxide" film). Figure 6a shows that the O_3 dissociative sticking coefficient, and hence the oxygen uptake, on the surface containing oxidized Sn is slower than on the oxygen-free alloy.

On the (2 × 2) alloy, the change in the AES oxygen uptake rate between $\Theta_O = 0.7-1.0$ coincides with a change in the shape of the O_2 TPD curves from broad to narrow that is indicative of a change in the oxygen chemical state from chemisorbed oxygen to PtO_x.

As shown in Figure 7a, oxygen uptake for the $\sqrt{3}$ surface initially proceeds relatively slowly with little change in the signals for Sn, Pt, or the Sn/Pt ratio. The O(506) signal increases more rapidly for O_3 exposures that produce $\Theta_O > 0.1$ up to Θ_O near 0.7, where the uptake slows again. Both Sn(430) and Pt(237) signals decrease over this range of oxygen concentrations, such that the Sn/Pt ratio increases about 40%. Figure 7b shows that while the O(KVV) and the Pt(NNO) peaks never shift appreciably, Sn(MNN) peak shifts lower by 1.6 eV (just as for the (2 × 2) alloy) at least by an oxygen concentration of

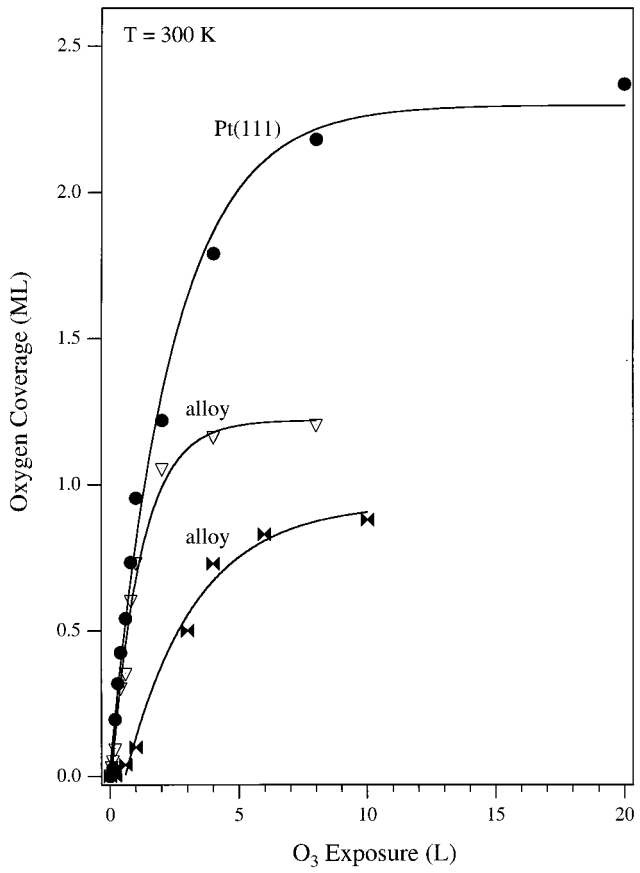

Figure 5. Oxygen uptake curves comparing the efficiency of O_3 exposures on Pt(111) and the (2 × 2)- and ($\sqrt{3}$x$\sqrt{3}$)R30°-Sn/Pt(111) alloys at 300 K.

$\Theta_O = 0.54$. Oxygen uptake is inhibited at larger oxygen coverages which also cause the formation of oxidized Sn.

Upon comparison to the corresponding TPD data of Figure 4, we see that $\Theta_O = 0.1-0.15$ is about the amount of oxygen that is required to saturate the O_2 desorption yield from the high-temperature state at 1078 K in TPD that we will later show is from SnO_x. The large decrease in the uptake rate as saturation coverage is approached corresponds to a change in the TPD spectra between $\Theta_O = 0.73-0.83$, where oxygen desorbs from a chemisorbed oxygen state on Pt to oxygen desorption from PtO_x.

Annealing experiments utilizing AES were also carried out in order to study further detailed changes in the surface composition and chemical state during heating in TPD. Figure 8a,b shows the changes in AES and LEED that occur during heating, starting with a saturation coverage of $\Theta_O = 1.2$ on the (2 × 2) alloy at 300 K. Heating to 700 K caused no large changes in the surface composition and structure and only a slight reduction in the O/Pt ratio was seen. O_2 desorption between 700 and 800 K caused a large decrease in the O(KVV) signal, a moderate increase in the Pt signal, and a small increase in the Sn signal. At temperatures above 800 K, the Pt signal is constant at the same intensity as that for the clean (2 × 2) alloy. Over the temperature range 800−1000 K, the Sn signal increases steadily to a maximum near 1000 K and then decreases at higher temperatures. The Sn/Pt ratio is increased by 27% following the adsorption of $\Theta_O = 1.2$ on the (2 × 2) alloy at 300 K, but this ratio returns to the clean alloy value upon heating to 800 K. Annealing to higher temperatures first increases the Sn/Pt ratio to a maximum value near 1000 K before the clean alloy surface value is recovered at 1100 K. The chemical shift of the

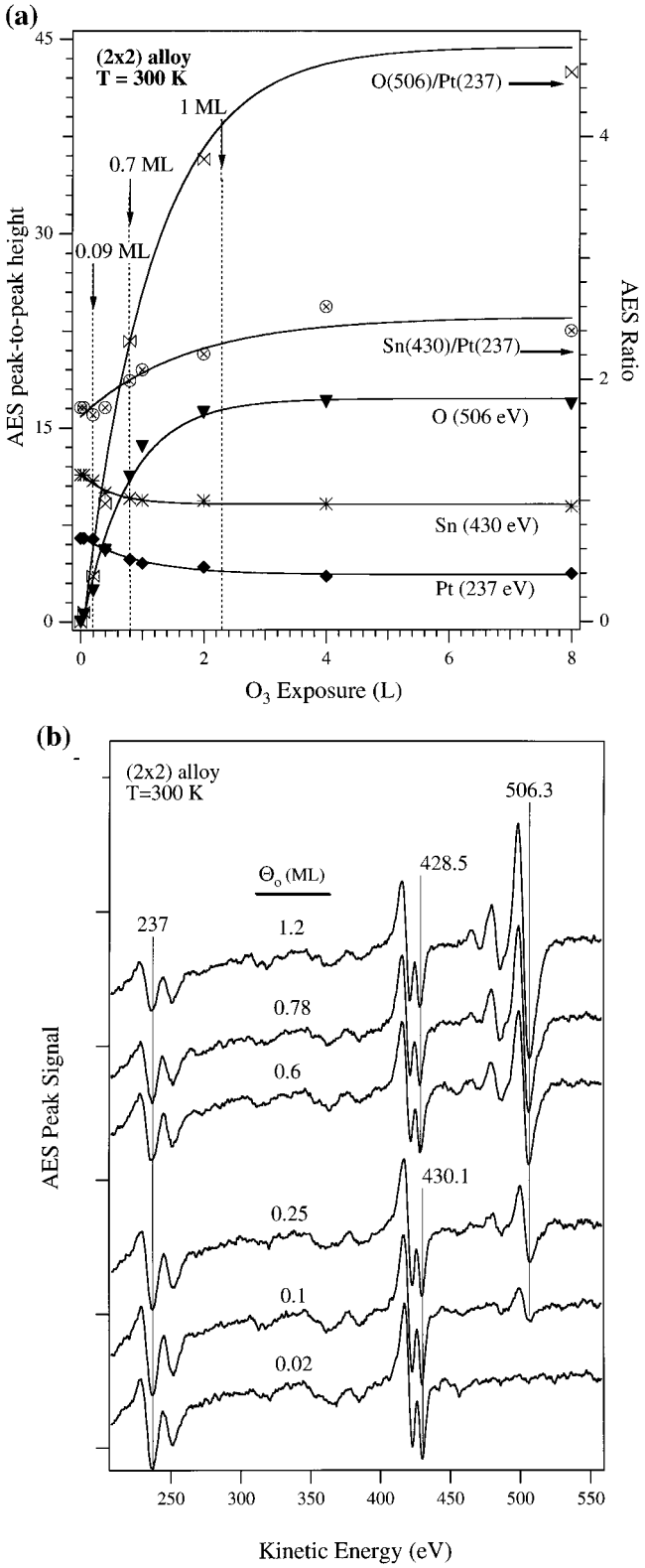

Figure 6. (a) AES peak-to-peak signal intensities at O(506 eV), Pt(237 eV), Sn(430 eV), along with the Sn(430 eV)/Pt(237 eV) and the O(506 eV)/Pt(237 eV) intensity ratios as a function of O_3 exposures on the (2 × 2)-Sn/Pt(111) surface alloy at 300 K. (b) AES spectra after increasing O_3 exposures on the (2 × 2)-Sn/Pt(111) surface alloy at 300 K. A shift of the Sn peak between 0.25 and 0.6 monolayer oxygen coverage indicates a change in the chemical state of Sn.

Sn AES peak that was induced by oxygen uptake to $\Theta_O = 1.2$ does not change until annealing temperatures larger than 800 K are reached, as shown in Figure 8b. At 900 K an intermediate position was observed, and after annealing to 1000 K to remove

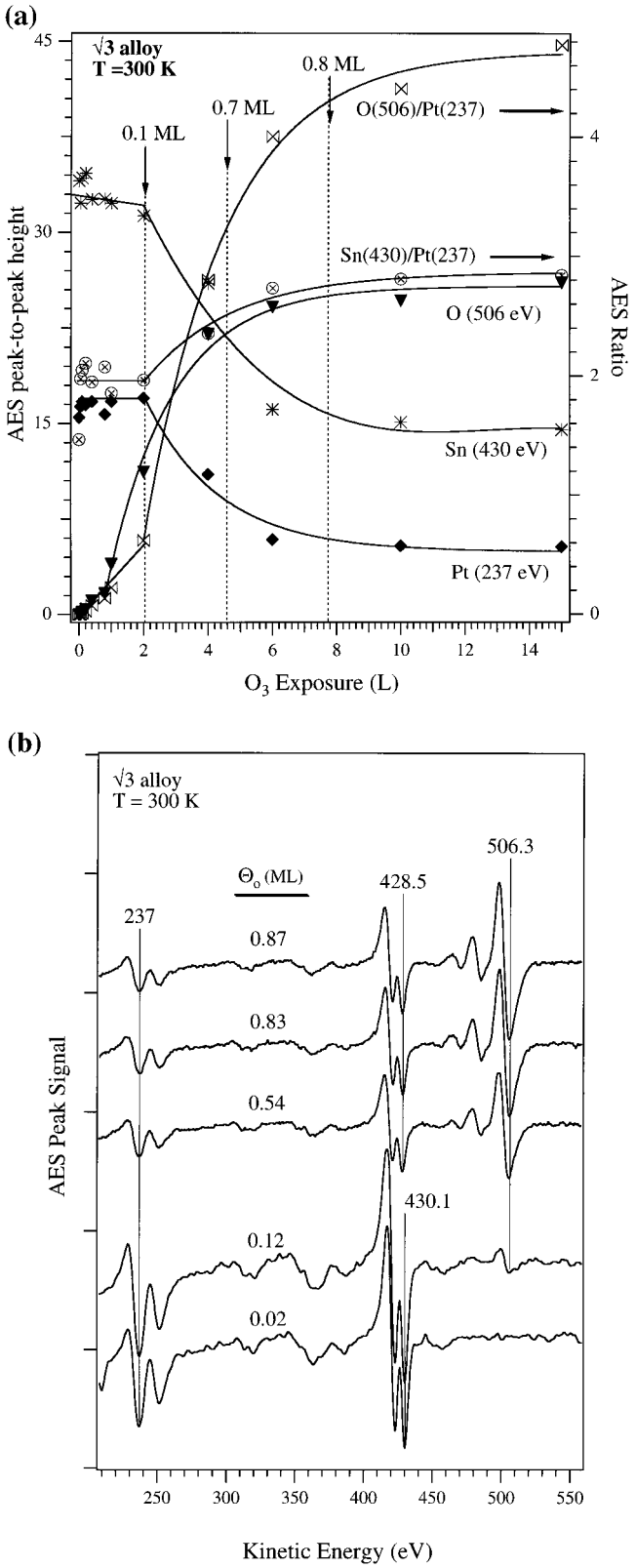

Figure 7. (a) AES peak-to-peak signal intensities at O(506 eV), Pt(237 eV), Sn(430 eV), along with the Sn(430 eV)/Pt(237 eV) and the O(506 eV)/Pt(237 eV) intensity ratios as a function of O_3 exposures on the ($\sqrt{3}$x$\sqrt{3}$)R30°-Sn/Pt(111) surface alloy at 300 K. (b) AES spectra after increasing O_3 exposures on the ($\sqrt{3}$x$\sqrt{3}$)R30°-Sn/Pt(111) surface alloy at 300 K. A shift of the Sn peak between 0.12 and 0.54 monolayer oxygen coverage indicates a change in the chemical state of Sn.

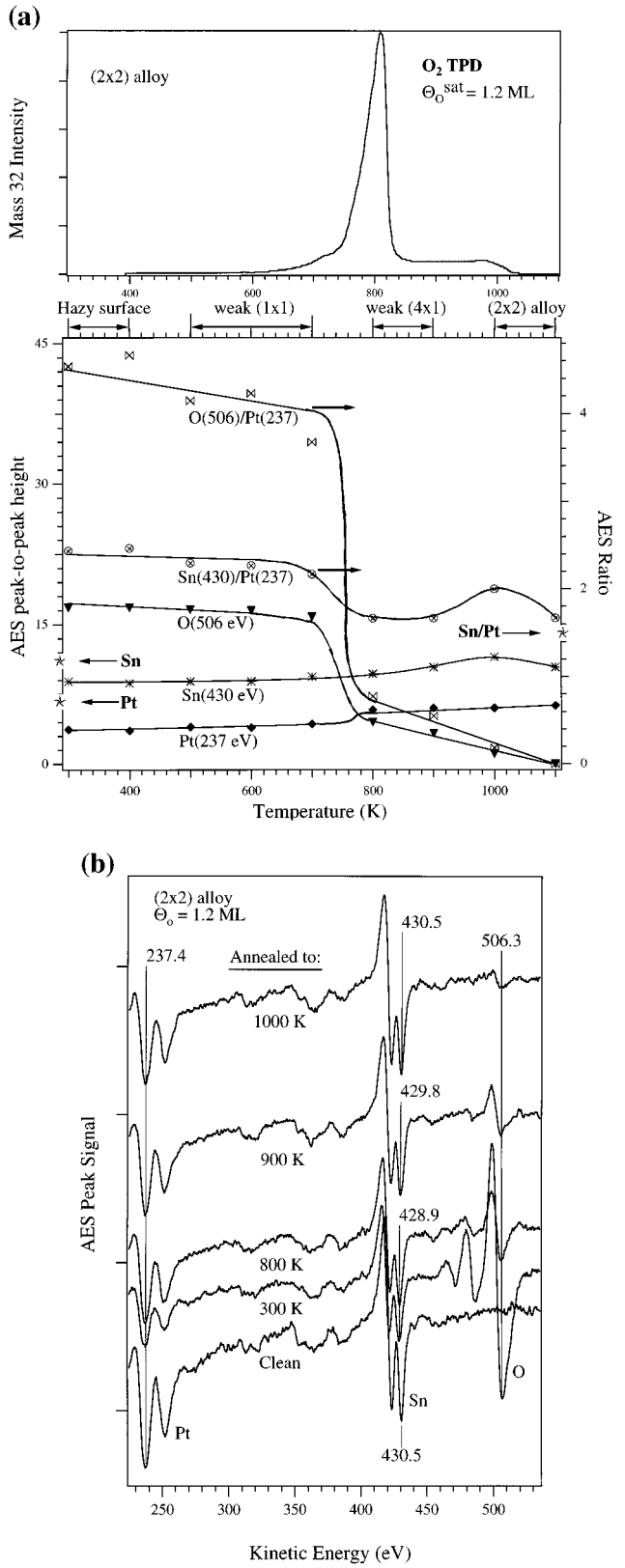

Figure 8. (a) AES signal intensities at O(506 eV), Pt(237 eV), Sn(430 eV), and the Sn(430 eV)/Pt(237 eV) and O(506 eV)/Pt(237 eV) ratios for increasing temperatures on the (2 × 2)-Sn/Pt(111) surface alloy. LEED changes observed during these temperature variations is also displayed. The O_2 TPD spectrum after an O_3 saturation dose is shown in the top panel. The Sn(430 eV) and Pt(237 eV) AES intensities along with the Sn(430 eV)/Pt(237 eV) ratio before oxidation are indicated on the vertical axes by "stars". (b) AES spectra after a saturation O_3 exposure on the (2 × 2)-Sn/Pt(111) alloy at 300 K was subsequently heated to increasingly higher temperatures. Shifts of the Sn peaks indicate changes in chemical state due to oxidation.

all oxygen, the Sn AES peak energy shifts back to that of the clean alloy. Taken together, Figure 8, parts a and b, establish that the large TPD peak at 820 K corresponds to desorption

from Pt sites and that desorption in the broad tail from 840 K to the peak at 1015 K corresponds to desorption from oxidized Sn. On this alloy, while an SnO_x overlayer is formed, this SnO_x overlayer does not cover extensively the Pt surface above 800 K because the Pt AES intensity returns to nearly the clean alloy value at 800 K. This conclusion is consistent with observations of only weak, new spots that are characteristic of low concentrations of small domains of an ordered SnO_x overlayer.

Figure 9, parts a and b, quantifies the changes in AES and LEED following dosing ozone on the $\sqrt{3}$ alloy at room temperature to produce a saturation oxygen coverage of $\Theta_O = 0.87$ and then increasing the temperature sequentially until reaching 1200 K. Oxygen uptake again increases the Sn/Pt ratio by 33%, and this ratio is nearly constant until 900 K where this ratio decreases following the large desorption peak of O_2. Heating to 1000 K causes a large increase in the Sn/Pt ratio, exceeding the value of that on the clean $\sqrt{3}$ alloy by 77%. Desorption of O_2 in the TPD peak at 1078 K causes a decrease in this ratio, and heating to 1200 K causes a significant reduction in the Sn signal and Sn/Pt ratio below that of the clean $\sqrt{3}$ alloy. The Sn/Pt ratio at 1200 K corresponds to that seen in Figure 8a for the clean (2×2) alloy. The chemical shifts observed for the Sn AES peak in Figure 9b parallel those discussed in Figure 8b. Taken together, Figure 9, parts a and b, establish that the large TPD peak at 820 K corresponds to desorption from Pt sites and that desorption in the peak at 1078 K corresponds to desorption from oxidized Sn.

Furthermore, the changes in AES that occur between 800 and 1000 K are consistent with the formation of a SnO_x overlayer that causes a new (4×1) LEED pattern to be superimposed on the $\sqrt{3}$ spots. Loss of all spots and a large background intensity characterized the disordered surface obtained initially after exposing a saturation dose of ozone on the surface at 300 K. After annealing at 500 K, the first faint (1×1) spots in LEED appeared. As the annealing temperature was increased, the (1×1) spots became brighter and $\sqrt{3}$ spots appeared. For annealing temperatures above 800 K, 1/4-order spots were observed, and we assign the observed LEED pattern to a superposition of three degenerate orientations of a (4×1) structure along with the ($\sqrt{3}$x$\sqrt{3}$)R30° structure. The LEED images along with further analysis of the SnO_x structure will be reported elsewhere.[62] AES and LEED confirm the formation of a well-ordered (2×2) alloy after desorbing all of the oxygen and heating to 1200 K. Annealing a $\sqrt{3}$ alloy in the absence of any oxygen in a vacuum to 1200 K never results in the formation of a (2×2) alloy.

Discussion

Ozone (O_3) is a very aggressive oxidant which leads to oxidation of Pt(111) under UHV conditions. Oxygen uptake from ozone exposures on Pt(111) at 300 K can be described as follows.[45] At low coverages ($\Theta_O \leq 0.25$), oxygen adatoms adsorb on 3-fold hollow sites and this leads to symmetric O_2 TPD peaks characteristic of second-order desorption kinetics. A (2×2)-O/Pt(111) structure was observed near $\Theta_O = 0.25$. Oxygen adatoms are formed for all Θ_O below 1, but the O_2 TPD peaks show a complex coverage dependence and shift about 200 K to lower temperatures as the coverage of oxygen increases. The large decrease in the O_2 desorption temperature arises from weakening the Pt−O bond because of lateral interactions within the oxygen adlayer. Once the concentration exceeds $\Theta_O = 1$, nucleation and growth of platinum oxide occurs at 300 K. This is characterized by sharp and narrow O_2 TPD peaks, which shift to higher temperatures and show

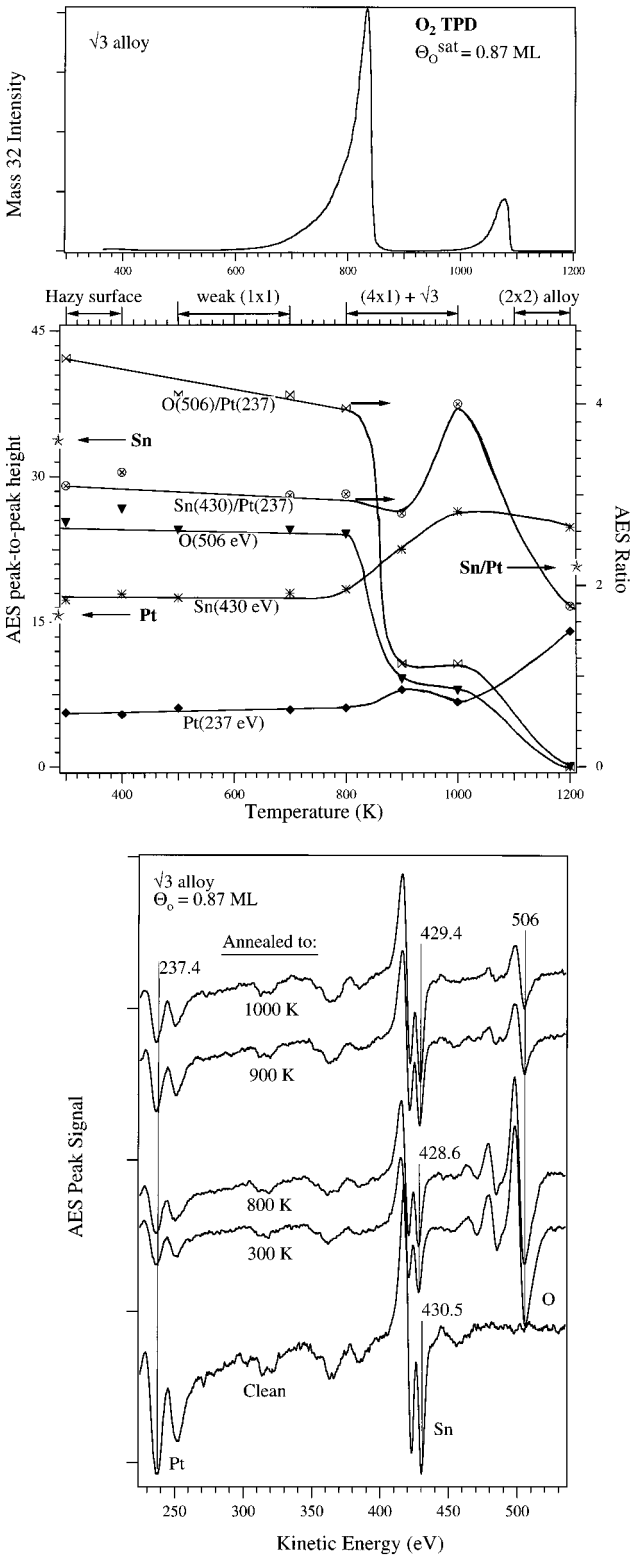

Figure 9. (a) AES signal intensities at O(506 eV), Pt(237 eV), Sn(430 eV), and the Sn(430 eV)/Pt(237 eV) and O(506 eV)/Pt(237 eV) ratios for increasing temperatures on the ($\sqrt{3}$x$\sqrt{3}$)R30° Sn/Pt(111) surface alloy. LEED changes observed during these temperature variations is also displayed. The O_2 TPD spectrum after an O_3 saturation dose is shown in the top panel. The Sn(430 eV) and Pt(237 eV) AES intensities along with the Sn(430 eV)/Pt(237 eV) ratio before oxidation are indicated on the vertical axes by "stars". (b) AES spectra after a saturation O_3 exposure on the ($\sqrt{3}$x$\sqrt{3}$)R30°-Sn/Pt(111) alloy at 300 K was subsequently heated to increasingly higher temperatures. Shifts of the Sn peaks indicate changes in chemical state due to oxidation.

undercutting with increasing coverages, and changes in the O(KVV) AES line shape. Saturation concentrations of oxygen (up to $\Theta_O = 2.4$) on Pt(111) at 300 K leads to disordered oxygen layers and loss of the Pt(111) LEED pattern. Annealing the oxidized Pt(111) surface to 1000 K regenerated the clean Pt(111) (1 × 1) pattern.

Even though kinetic effects eliminate dissociative O_2 chemisorption on the (2 × 2) and $\sqrt{3}$ Sn/Pt(111) surface alloys, O_3 exposures to these surfaces at 300 K leads to oxygen uptake and oxidation of the alloys. Following an integrated discussion of our TPD, AES, and LEED observations, we will propose a model for this chemistry on the two Pt−Sn surface alloys as well.

Small coverages ($\Theta_O < 0.3$) of oxygen produced by ozone dissociation on the two alloys at 300 K did not induce any change in the Sn(MNN) AES peak kinetic energy. Thus, Pt atoms are probably involved in bonding oxygen adatoms from ozone dissociation on the alloy surfaces at low temperatures. However, we obtain O_2 TPD peaks that desorb at very high temperature compared to those from Pt(111) that occur at 814−675 K. The O_2 peak in TPD at 960−1015 K on the (2 × 2) alloy and 1002−1078 K on the $\sqrt{3}$ alloy is assigned to O_2 desorption from the decomposition of SnO_x that is formed by heating the surface during TPD. Tin oxide is formed at high temperature because of the increase in diffusion rates and the migration of oxygen from Pt to Sn sites since Sn has a higher affinity than Pt toward oxygen.[63] The increase in the O_2 desorption temperature compared to that on Pt(111) can be attributed to the difference in the metal−oxygen bond strengths, with Sn−O bonding being stronger than that for Pt−O. In the gas-phase diatomics PtO and SnO, D(Pt−O) = 93.6 kcal/mol and D(Sn−O) = 127 kcal/mol.[63] Using ΔH_f^o values for PtO_2(g), SnO(s), and SnO_2(s), we calculate that D(Pt−O) = 80 kcal/mol and D(Sn−O) = 126.5 and 128.5 kcal/mol, respectively. Redhead analysis[64] of the TPD data indicates that the O_2 desorption activation energy E_d at low oxygen coverages increases from 51 kcal/mol on Pt(111) to 67 and 75 kcal/mol on the (2 × 2) and $\sqrt{3}$ Sn/Pt(111) surface alloys, respectively. From these values, we find D(Pt−O) = 85 and D(Sn−O) = 93 and 97 kcal/mol for the (2 × 2) and $\sqrt{3}$ alloys, respectively. The shift in the O_2 desorption peak derived from SnO_x to higher temperatures with increasing oxygen coverages shows that the SnO_x phase acquires more stability as the oxygen coverage increases on the alloy surfaces. This could be attributed to increasing lateral attractive interactions that occur with increasing SnO_x particle size or simply due to the Kelvin effect of decreasing vapor pressure with increasing particle size.[65] At these small oxygen concentrations, we do not expect that diffusion of oxygen to the surface is rate-limiting.

For medium coverages, ($0.3 \leq \Theta_O \leq 0.7$), oxidation of Sn in the (2 × 2) and $\sqrt{3}$ alloys at 300 K leads to the formation of Pt−O−Sn bonds. The evidence for this in our work is a shift of 1.6 eV in the Sn(MNN) AES peak. The existence of Pt−O−Sn bonds on bulk alloys was demonstrated in a number of papers by Hoflund and co-workers.[66−68] Heating the surface alloys during TPD formed an oxygen chemisorbed state on Pt and a tin oxide state. This change is reflected as two regimes in the O_2 desorption profile: a high-temperature feature from decomposition of SnO_x particles and lower temperature peaks from chemisorbed oxygen on Pt sites. As Θ_O increases, the Pt-derived O_2 TPD peaks shift to lower temperature because of a reduction in the Pt−O bond energy, consistent with either higher lateral interactions in the oxygen adlayer or population of more weakly bound sites. At $\Theta_O \sim 0.7$, O_2 desorption from the alloy surfaces occurs in a much narrower temperature range (100 K) than on Pt(111) (150 K), and the O_2 desorption temperature is shifted to ~730 K on the alloy surfaces from 634 K on Pt(111). Hence, the oxygen adlayer is stabilized on the alloys over that on Pt(111) and this would be consistent with smaller repulsive interactions between oxygen adatoms on the alloys.

Near saturation oxygen coverages that were produced by large ozone exposures, oxidation of Sn on the (2 × 2) and $\sqrt{3}$ alloy surfaces at room temperature leads to the formation of Pt−O−Sn bonds as indicated by a Sn(MNN) AES peak shift of 1.6 eV. These surfaces are disordered at room temperature, i.e., there were no LEED spots. O_2 TPD from both alloys shows high-temperature peaks (>815 K) due to SnO_x decomposition and sharp, narrow peaks near 800 K from PtO_x decomposition. These latter TPD peaks shift from 707 K on Pt(111) to 817 K on the (2 × 2) alloy and to 835 K on the $\sqrt{3}$ surface alloy. This reveals an increase in the thermal stability of PtO_x in the presence of Sn or SnO_x at the surface. Furthermore, Sn facilitates PtO_x formation as well, and so an O_2 TPD peak characteristic of PtO_x decomposition was observed for $\Theta_O = 1$ on the (2 × 2) alloy and $\Theta_O = 0.8$ on the $\sqrt{3}$ surface alloy, while only desorption from chemisorbed states was observed at $\Theta_O = 0.95$ on P(111). On the other hand, Pt plays the opposite role in the formation and decomposition temperature of SnO_x. Only low O:Sn stoichiometries (less than 1:1) were obtained from oxidation of the surface alloys, and O_2 desorption from SnO_x decomposition occurs at lower temperatures of 100−200 K on the alloys compared to the O_2 desorption obtained from a thick layer of SnO_x prepared by oxidation of a thick Sn film on Pt(100).[51,52]

If saturation coverages of $\Theta_O = 1.2$ on the (2 × 2) alloy and $\Theta_O = 0.87$ on the $\sqrt{3}$ surface alloy are annealed above 800 K, a (4 × 1) LEED pattern was observed. We attribute this structure to the ordering of islands of SnO_x. Further heating regenerates a (2 × 2) LEED pattern characteristic of the (2 × 2) surface alloy after the complete desorption of oxygen at 1100 K, independent of which alloy was formed initially prior to oxidation.

The following picture emerges for the ozone oxidation of the two Pt−Sn surface alloys. Small ozone exposures on the alloys at room temperature produce oxygen adatoms bound to Pt which migrate to form SnO_x at temperatures above 800 K. Even at room temperature, high oxygen concentrations lead to Sn−O bonding in addition to chemisorbed oxygen on Pt or PtO_x particles at the highest oxygen coverages. At high temperatures (T > 800 K), an SnO_x overlayer can be formed (most clearly visible on the $\sqrt{3}$ alloy) which decomposes below 1100 K to regenerate the (2 × 2)-Sn/Pt(111) surface alloy on either of the two surface alloys.

To quantify the amount of oxidized Sn on the (2 × 2) and $\sqrt{3}$ alloys, we measured the area of the high-temperature peaks in the O_2 TPD spectra. These were calibrated to Θ_O by utilizing the O_2 TPD area obtained from dosing O_2 on Pt(111) at 300 K to give $\Theta_O = 0.25$. On the (2 × 2) alloy, the amount of oxygen liberated from SnO_x decomposition is $\Theta_O = 0.1-0.2$ (depending on the amount of desorption between 850 and 950 K attributed to SnO_x decomposition), and is $\Theta_O = 0.1-0.15$ on the $\sqrt{3}$ alloy. This amount is obviously not sufficient to oxidize all the Sn present in the alloy to SnO or SnO_2, and thus in all cases some alloyed Sn remained. Formation of an SnO_2 adlayer at the surface using this amount of oxygen requires dealloying of $\Theta_{Sn} \sim 0.07$. This consumes about one-third of the surface Sn in the (2 × 2) alloy and the brief heating during TPD to decompose the Sn oxide does not regenerate a high-quality (2 × 2) surface alloy. On the other hand, this only changes the surface Sn

concentration in the $\sqrt{3}$ alloy from $\Theta_{Sn} = 0.33$ to approximately $\Theta_{Sn} = 0.25$, which is just that required for the formation of a high-quality (2×2) surface alloy.

There is precedence for proposing the formation of a SnO_2 adlayer in our work. Formation of an SnO_2 ring was detected around the original intermetallic Pt−Sn particles upon annealing oxidized Pt−Sn particles grown on thin planar amorphous SiO_2.[69] Also, annealing oxidized Sn/Au(111) alloy surfaces[70,71] produced a c(4×2) LEED pattern attributed to a periodic arrangement of SnO_2 on the Sn/Au(111) alloy surface. SnO_2 formed on these surfaces is expected to have a lower surface free energy than the intermetallic Pt−Sn compound, and Sn is more mobile than Pt and therefore can easily migrate on the surface to react with $O_{(a)}$.[72] With the data reported here, it is difficult to differentiate directly between the two stable oxides, i.e., stannous oxide, SnO, and stannic oxide, SnO_2.[28,30] The formation of a thin oxide layer on a relatively large concentration of unreacted, alloyed tin complicates elucidation of a clear chemical shift for the Sn(M_4,$N_{4,5}N_{4,5}$) AES transition for the Sn oxide formed.

XPS and ELS are powerful methods for assigning chemical states, and we need additional studies to provide better information about the chemical nature of Sn at different oxygen concentrations and temperatures. We have carried out two independent oxidation studies of Sn/Pt(111)[73] and Sn/Pt(100)[50,51] surface alloys using XPS. Dosing a high pressure of oxygen ($P_{O_2} = 1$ Torr) on the Sn/Pt(111)[73] alloys at 300 K oxidized the surface and caused a Sn($3d_{5/2}$) peak shift of +0.55 eV relative to that on the alloy. Subsequently annealing this surface in a vacuum to 1000 K caused an additional shift in the Sn($3d_{5/2}$) peak, such that the peak shift was +1.1 eV relative to the alloy. Also, during studies of the oxidation of Sn/Pt(100)[50,51] alloys using O_3 in UHV, the same Sn(MNN) AES peak shift (1.6 eV) was observed as we report herein for Sn/Pt(111) surface alloys. However, two different Sn($3d_{5/2}$) peak shifts of 0.5 and 1.2 eV in XPS were observed for a saturation coverage of oxygen after dosing at 300 K and after subsequent annealing to 1000 K, respectively. These results are consistent with the findings of Hoflund and co-workers[21,23,24] on Pt_3Sn bulk alloys and support our assignments of the oxidation of Sn at 300 K and the formation of SnO_x at high temperatures.

Finally, our conclusions about the Pt-enhanced reduction of small Sn oxide particles is consistent with prior studies on bulk samples. Annealing treatments carried out on platinized tin oxide[74] lead to the formation of a Pt−Sn alloy at 720 K whereas annealing tin oxide films at 720 K did not result in the reduction of tin oxide to metallic tin.[75,76] Our observation of the Sn-enhanced stability of small Pt oxide particles has not been discussed in prior work.

Conclusion

Even though the (2×2) and $\sqrt{3}$ Sn/Pt surface alloys are less reactive than Pt(111) and the dissociative chemisorption of O_2 under UHV conditions is eliminated, oxidation of these alloys can be achieved under UHV conditions by using ozone (O_3). Dosing ozone at room temperature on these two ordered Sn/Pt surface alloys resulted initially in the formation of chemisorbed oxygen at Sn sites, but probably utilizing Pt sites for dissociation of ozone. This is a strong Sn−O interaction that results in a 1.6 eV shift in the Sn(MNN) AES peak, but is not yet representative of an "oxide" film. Oxygen adatoms are chemisorbed on Pt sites at large oxygen coverages and, at the highest oxygen coverages, PtO_x is formed. Nucleation of PtO_x particles was identified by the characteristically sharp (35 K) TPD curves and by the O_2 TPD peak temperature which is close to that for the decomposition of PtO_x particles on the Pt(111) surface. Heating ($T > 800$ K) these oxygen-covered alloy surfaces causes the nucleation and formation of SnO_x, which gives a well-ordered (4×1) LEED pattern on both alloy surfaces at $T \geq 900$ K. Oxidized Sn is reduced and the (2×2)-Sn/Pt(111) surface alloy is reformed after vacuum annealing to desorb all oxygen from the surface after oxidation of either alloy. A key chemical finding is that the presence of Sn at the Pt surface enhanced the formation of PtO_x from adsorbed oxygen and stabilized these particles against reduction. Also, the proximity of Pt that results from oxidation of the Pt−Sn alloys lowers the thermal decomposition temperature of SnO_x.

Acknowledgment. This work was supported by the Division of Chemical Sciences, Office of Basic Energy Sciences, U.S. Department of Energy.

References and Notes

(1) Karpinski, Z.; Clarke, J. K. A. *J. Chem. Soc., Faraday Trans.* **1975**, *271*, 893.
(2) Davis, B. H. *J. Catal.* **1977**, *46*, 348.
(3) Burch, R.; Garla, L. C. *J. Catal.* **1981**, *71*, 360.
(4) Srabo, G. L. In *Metal-Support and Metal-Additive Effects in Catalysis*; Imelik, B., et al., Eds.; Elsevier: Amsterdam/New York, 1982.
(5) Cortright, R. D.; Dumesic, J. A. *J. Catal.* **1995**, *157*, 576.
(6) Cathro, K. J. *J. Electrochem. Soc.* **1969**, *116*, 1608.
(7) Janssen, M. M. P.; Moolhusyen, J. *Electrochim. Acta* **1976**, *21*, 861.
(8) Andrew, M. R.; Dury, J. S.; McNicol, B. D.; Pinnington, C.; Short, R. T. *J. Appl. Electrochem.* **1976**, *6*, 99.
(9) Stark, D.; Cross, A. P. H.; Steward, G. J. *J. Phys. E: Sci. Instrum.* **1983**, *16*, 158.
(10) Hoflund, G. B.; Upchurch, B. T.; Keilin, E. J.; Schryer, D. R. *Catal. Lett.* **1995**, *31*, 133.
(11) Hoflund, G. B.; Gardner, S. D.; Schryer, D. R.; Upchurch, B. T.; Keilin, E. J. *Langmuir* **1995**, *11*, 3431.
(12) Gasteiger, H. A.; Markovic, N. M.; Ross, P. N., Jr. *J. Phys. Chem.* **1995**, *99*, 8495.
(13) Gasteiger, H. A.; Markovic, N. M.; Ross, P. N., Jr. *Catal. Lett.* **1996**, *36*, 1.
(14) Wang, K.; Gasteiger, H. A.; Markovic, N. M.; Ross, P. N., Jr. *Electrochim. Acta* **1996**, *41*, 2587.
(15) Markovic, N. M.; Widelov, A.; Ross, P. N., Jr. *Catal. Lett.* **1997**, *43*, 161.
(16) Morimoto, Y.; Yeager, E. B. *J. Electroanal. Chem.* **1998**, *441*, 77.
(17) Bouwman, R.; Toneman, L. H.; Holsher, A. A. *Surf. Sci.* **1973**, *35*, 8.
(18) Bouwman, R.; Biloen, P. *Anal. Chem.* **1974**, *46*, 136.
(19) Bouwman, R.; Biloen, P. *Surf. Sci.* **1974**, *41*, 348.
(20) Biloen, P.; Bouwman, R.; VanSanten, R. A.; Brongerman, H. H. *Appl. Surf. Sci.* **1979**, *2*, 532.
(21) Hoflund, G. B.; Asbury, D. A.; Kirszensztejn, P.; Laitinen, H. A. *Surf. Interface Anal.* **1986**, *9*, 169.
(22) Gardner, S. D.; Hoflund, G. B.; Davidson, M. R.; Schryer, D. R. *J. Catal.* **1989**, *115*, 132.
(23) Asbury, D. A.; Hoflund, G. B. *Surf. Sci.* **1988**, *199*, 552.
(24) Gardner, S. D.; Hoflund, G. B.; Schryer, D. R. *J. Catal.* **1989**, *119*, 179.
(25) Unger, W.; Marton, D. *Surf. Sci.* **1989**, *218*, L467.
(26) Rotermund, H. H.; Penka, V.; DeLouise, L. A.; Brundle, C. R. *J. Vac. Technol. A* **1987**, *5* (4), 1198.
(27) Asbury, D. A.; Hoflund, G. B. *J. Vac. Sci. Technol. A* **1987**, *5* (4), 1132.
(28) Holm, R.; Storp, S. *Appl. Phys.* **1976**, *9*, 217.
(29) Ansell, R. O.; Dickinson, T.; Povey, A. F.; Sherwood, P. M. A. *J. Electron Spectrosc. Relat. Phenom.* **1977**, *11*, 301.
(30) Sen, S. K.; Sen, S.; Bauer, L. *Thin Solid Films* **1981**, *82*, 157.
(31) Bevolo, A. J.; VerHoeven, J. D.; Noack, M. *Surf. Sci.* **1983**, *134*, 499.
(32) Cox, D. F.; Hoflund, G. B. *Surf. Sci.* **1985**, *151*, 202.
(33) Sherwood, P. M. A. *Phys. Rev. B* **1990**, *41*, 10151.
(34) Ingo, G. M.; Giorgi, L.; Zacchetti, N.; Azzeri, N. *Corrosion Sci.* **1991**, *20*, 361.
(35) Hoflund, G. B.; Corallo, G. R. *Phys. Rev. B* **1992**, *46*, 7110.
(36) Themlin, J. M.; Chtaib, M.; Henrad, L.; Lambin, P.; Darville, J.; Gilles, J. M. *Phys. Rev. B* **1992**, *46*, 2460.

(37) Padova, P. D.; Fanfoni, M.; Larcripete, R.; Mangiantini, M.; Priori, S.; Perfetti, P. *Surf. Sci.* **1994**, *313*, 379, and references therein..

(38) Gaggiotti, G.; Galdikas, A.; Kaciulis, S.; Mattogno, G.; Setkus, A. *J. Appl. Phys*. **1994**, *76*, 4467.

(39) Lamy-Pitara, E.; Elouazzani-Benhim, L.; Barbier, J.; Cahorean, M.; Caisso, J. *J. Electroanal. Chem*. **1994**, *372*, 233.

(40) Kover, L.; Moretti, G.; Kovacs, Zs.; Sanjines, R.; Cserny, I.; Margritondo, G.; Palimkas, J.; Adachi, H. *J. Vac. Sci. Technol. A* **1995**, *13* (3), 1382.

(41) Merlen, E.; Beccat, P.; Bertolini, J. C.; Delichere, P.; Bidillon, B. *J. Catal*. **1996**, *159*, 178.

(42) H_2O coadsorption from the background gases can be minimized (effectively eliminated) by low-pressure dosing of O_3 with a directed beam doser. Water formation due to surface reactions with coadsorbed hydrogen do not occur on these Pt−Sn surface alloys because the dissociative sticking coefficient of H_2 on these surface is nearly zero.[43.]

(43) Paffet, M. T.; Gebhard, S. C.; Windham, R. G.; Koel, B. E. *J. Phys. Chem*. **1990**, *94*, 6831.

(44) Saliba, N. A.; Holmes, D.; Koel, B. E. *Surf. Sci.* **1998**, *410*, 270.

(45) Saliba, N. A.; Tsai, Y. L.; Koel, B. E. *Surf. Sci*., in press.

(46) Beck, D.; Saliba, N. A.; Baur, C.; Koel, B. E., in preparation..

(47) Sales, B. C.; Turner, J. E.; Maple, M. B. *Surf. Sci*. **1981**, *112*, 272.

(48) Gland, J. L.; Sexton, B. A.; Fisher, G. B. *Surf. Sci*. **1980**, *95*, 587.

(49) Niehus, H.; Comsa, G. *Surf. Sci.* **1980**, *93*, L147.

(50) Saliba, N. A.; Beck, D.; Baur, C.; Koel, B. E., in preparation.

(51) Saliba, N. A.; Beck, D.; Baur, C.; Koel, B. E., in preparation.

(52) Windham, R. G.; Bartram, M. E.; Koel, B. E. *J. Phys. Chem*. **1988**, *92*, 2862.

(53) Gland, J. L. *Surf. Sci*. **1980**, *93*, 487.

(54) Paffett, M. T.; Windham, R. G. *Surf. Sci*. **1989**, *208*, 34.

(55) Overbury, S. H.; Mullins, D. R.; Paffett, M. T.; Koel, B. E. *Surf. Sci*. **1991**, *254*, 45.

(56) Atrei, A.; Bardi, U.; Rovida, G.; Torrini, M.; Zamazzi, E.; Ross, P. N. *Phys. Rev. B* **1992**, *46*, 1649.

(57) Galeotti, M.; Atrei, A.; Bardi, U.; Rovida, G.; Torrini, M. *Surf. Sci.* **1994**, *313*, 349.

(58) Campbell, C. T.; Ertl, G.; Kupers, H.; Segner, J. *Surf. Sci*. **1981**, *107*, 220.

(59) Eisert, F.; Elg, A. P.; Rosen, A. *Appl. Phys. A* **1995**, *60*, 209.

(60) Elg, A. P.; Eisert, F.; Rosen, A. *Surf. Sci.* **1997**, *382*, 57.

(61) Parker, D. H.; Bartram, M. E.; Koel, B. E. *Surf. Sci*. **1990**, *233*, 65.

(62) Voss, M.; Busse, H.; Koel, B. E., in preparation.

(63) Lide, D. R *Handbook of Chemistry and Physics*, 73rd ed.; CRC Press Inc.: Boca Raton, FL, 1992.

(64) Redhead, P. A. *Vacuum* **1962**, *12*, 203.

(65) Adamson, A. W.; Gast, A. P. *Physical Chemistry of Surfaces*, 6th ed.; Wiley & Sons: New York, 1997; Chapter 3.

(66) Cox, D. F.; Hoflund, G. B.; Laitinen, H. A. *Langmuir* **1985**, *1*, 269.

(67) Hoflund, G. B.; Asbury, D. A.; Gilbert, R. E. *Thin Solid Films* **1985**, *129*, 139.

(68) Drawdy, J. E.; Hoflund, G. B.; Davidson, M. R.; Upchurch, B. T.; Schryer, D. R. *Surf. Interface Anal*. **1992**, *19*, 559.

(69) Chojnacki, T. P.; Schmidt, L. D. *J. Catal.* **1991**, *129*, 473.

(70) Zhang, Y.; Slavin, A. J. *J. Vac. Sci. Technol. A* **1992**, *10*, 2371.

(71) Zhang, Y.; Slavin, A. J. *Phys. Rev. B.* **1994**, *49*, 2005.

(72) Wagner, C. D.; Biloen, P. *Surf. Sci.* **1973**, *35*, 82.

(73) Jerdev, D.; Saliba, N. A.; Koel, B. E., in preparation.

(74) Gardner, S. D.; Hoflund, G. B.; Davidson, M. R.; Schryer, D. R. *J. Catal.* **1989**, *115*, 132.

(75) Hoflund, G. B.; Cox, D. F.; Woodson, G. L.; Laitinen, H. A. *Appl. Surf. Sci*. **1982**−**1983**, *14*, 281.

(76) Cox, D. F.; Hoflund, G. B.; Laitinen, H. A. *Appl. Surf. Sci.* **1984**, *20*, 30.